Dislocation Glides in Granular Media

Fumiaki Nakai,[1,*] Takashi Uneyama,[2] Yuto Sasaki,[1] Kiwamu Yoshii,[3] and Hiroaki Katsuragi[1]
[1]Department of Earth and Space Science, Osaka University, 1-1 Machikaneyama, Toyonaka 560-0043, Japan
[2]Department of Materials Physics, Graduate School of Engineering, Nagoya University, Furo-cho, Chikusa, Nagoya 464-8603, Japan
[3]Department of Applied Physics, Tokyo University of Science, 6-3-1, Nijuku, Katsushika, Tokyo, 125-8585, Japan

(Received 29 October 2024; revised 20 February 2025; accepted 2 June 2025; published 23 July 2025)

Atomic crystals with dislocations deform plastically at low stresses via dislocation glide. Whether dislocation glide occurs in macroscopic frictional granular media remains unknown. We simulate structural and rheological responses of a granular crystal with an edge dislocation. We discover that dislocation glide occurs at low interparticle friction coefficients, whereas at high friction, the crystal order breaks down. When the dislocation glide occurs, the yield stress is markedly lower than in dislocation-free crystals and varies linearly with the interparticle friction coefficient. The linear dependence arises from both the elastic barrier associated with the Peierls stress and the interparticle friction slip criteria.

DOI: 10.1103/7g7s-c157

Introduction—Microscopic crystals generally contain line defects known as dislocations and undergo plastic deformation at stress levels several orders of magnitude lower than those predicted by uniform deformation models [1–10]. This low stress, known as the Peierls stress, results from successive local dislocation glides within the crystal, as presented in Fig. 1, a process analogous to inchworm movement [8,11]. Dislocations are classified as edge dislocations when the dislocation line is perpendicular to the Burgers vector and as screw dislocations when they are parallel. Both edge and screw dislocations result in a wide range of plastic deformations [8,12]. Based on its physical origin, dislocation glide is not necessarily limited to microscopic systems. Nevertheless, in macroscopic systems consisting of particles several millimeters or larger, dislocation glides have rarely been observed except in specific cases.

Bragg, Nye [13,14], and Lomer [15,16] created a macroscopic two-dimensional crystal using bubbles with uniform diameters of approximately 0.5 mm floating on water. Under deformation, edge dislocations in this bubble crystal exhibit gliding behavior similar to that observed in microscopic crystals. Subsequent studies have further confirmed the presence of dislocation glide in bubble systems [17,18]. Despite these observations in bubble systems, dislocation glide remains unreported in other macroscopic systems, even though the deformation of macroscopic granular crystals has been extensively studied [19–25]. As such, the conditions necessary for the emergence of dislocation glide in macroscopic granular systems have remained unclear. Given that bubbles floating on water can be considered a frictionless granular medium (interparticle friction coefficient $\mu = 0$), a fundamental question arises: do dislocation glide and its associated low yield stress occur in frictional granular media ($\mu > 0$)? If so, how does interparticle friction affect the yielding rheology in granular crystals with a dislocation?

To address these issues, we consider a model system (see Fig. 2) inspired by the fundamental theory of atomic-scale dislocation glide [1–9]. Using the discrete element method (DEM) [26–30], we investigate the structural and rheological responses of the two-dimensional hexagonal crystal containing an edge dislocation under shear, focusing on the effects of interparticle friction coefficient μ. This Letter reports two key findings: (i) dislocation glide (characterized by Orowan's theory, see Fig. 1) emerges at low interparticle friction ($\mu \lesssim 0.1$) but not at high μ due to crystal breakage;

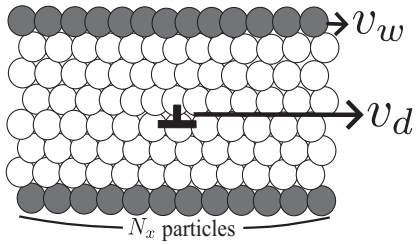

FIG. 1. Schematic of dislocation glide: the propagation of inchwormlike local deformation through the crystal [1–9]. The dislocation presented by $\perp$ moves with velocity $v_d = N_x v_w$ in response to wall velocity v_w, following Orowan's theory [8]. This deformation mechanism leads to lower yield stress, called Peierls stress at atomic scale [1,2,9], compared to perfect crystals.

*Contact author: fumiaki.nakai@ess.sci.osaka-u.ac.jp

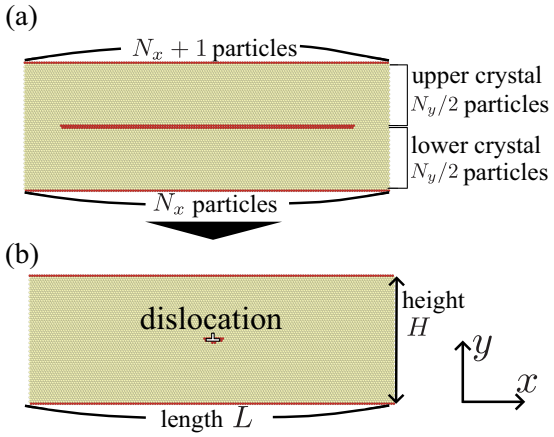

FIG. 2. System configuration of frictional granular particles. (a) Initial particle arrangement in a two-dimensional hexagonal lattice. The upper and lower crystals contain $(N_x + 1)N_y/2$ and $N_xN_y/2$ particles ($N_x = 150$, $N_y = 60$), respectively. Particles with six contacting neighbors appear yellow; all others appear red. Periodic boundary conditions apply along the x axis, with wall particles at top and bottom confining the bulk. The system width is $L = N_x\alpha d$ with $\alpha = 0.95$ being the lattice parameter. The system height $H = \sqrt{3}(N_y + 1)\alpha d/2$ is the distance between the centers of the top and bottom wall particles. (b) System relaxed with fixed H and L under a frictionless condition ($\mu = 0$), achieving a force-balanced state. This process creates a single dislocation at the center presented by a symbol $\perp$. Once the force-balanced state is achieved, interparticle friction μ is set to a target value, and shear is applied by moving the top wall along the x axis with fixed H and L.

(ii) when dislocation glide occurs, the yield stress σ_Y is notably lower than that of dislocation-free crystals and varies linearly with μ, reflecting the elastic barrier associated with the Peierls stress and interparticle friction. The gliding behavior and the low yield stress are characteristics of dislocation glide, which are absent in both amorphous and dislocation-free crystalline granular media. The observation of dislocation glide in granular media opens new avenues in materials sciences, fostering interdisciplinary research that bridges the gap between microscopic crystals and macroscopic materials.

Methodology overview—This study employs the DEM [26,30–32] implemented in LAMMPS [33] to simulate the dynamics of frictional granular particles. The system consists of a two-dimensional arrangement of bulk particles with periodic boundary conditions along the x axis and wall particles confining the bulk along the y axis. The diameter and mass density of the particle are $d = 1$ mm and $\rho = 1000$ kg/m^3, respectively. Material parameters are derived from elastomer properties [34,35], with particles having a Young's modulus $E = 1$ MPa and Poisson's ratio $\nu = 0.45$ (realistic parameters are used to demonstrate that the novel phenomena presented afterward occur under realistic conditions). Particle interactions are calculated using the Hertz-Mindlin-Tsuji contact model [28], accounting for normal and tangential forces between particles. We apply Coulomb's law of friction, with interparticle friction coefficients μ ranging from 0 to 1.

A key methodological advance is the introduction of a dislocation into the granular crystal, guided by atomic dislocation theory [1–10], as shown in Fig. 2. We achieve this by constructing an initial state with slightly different lattice vectors for the upper and lower system halves, containing $(N_x + 1)N_y/2$ and $N_xN_y/2$ particles, respectively, with numbers $N_x = 150$ and $N_y = 60$, resulting in a one-unit lattice misalignment across the interface [see Fig. 2(a)]. The system then relaxes while maintaining a fixed length $L = N_x\alpha d$ and height $H = \sqrt{3}(N_y + 1)\alpha d/2$, with lattice parameter $\alpha = 0.95$ [see Fig. 2(b)]. This force-balanced state with a single dislocation serves as the initial state for all subsequent analyses. Applying the constant shear rate of $\dot{\gamma} = 10^{-3}$ s^{-1} by moving the top wall with a velocity $v_w = \dot{\gamma}H$ along the x axis, we analyze the structural changes and rheological responses. Complete details of the simulation methodology are provided in Supplemental Material [36].

Results—The structural response to shear qualitatively varies with μ [see Fig. 3(a)]. In the frictionless case ($\mu = 0$), the dislocation site glides successively without disrupting crystal order. This gliding behavior persists even for weak but finite interparticle friction $\mu \lesssim 0.1$. The observed dislocation glide appears similar to that on the atomic scale [37]. In contrast, at $\mu \gtrsim 0.15$, the hexagonal structure partially breaks, and the dislocation glide ceases. The trajectories of the upper-side particles initially located at the interface exhibit different types of motion with respect to μ, as shown in Fig. 3(b). Colors indicate contact number Z, with $Z = 6$ for local hexagonal arrangement and $Z \neq 6$ otherwise. At $\mu \lesssim 0.1$, a continuous red line appears, signifying dislocation glide. The dislocation traverses the system with period $\gamma H/\alpha d = 1$, independent of μ. This period matches Orowan's theory [8], which results from a simple geometrical consideration: the dislocation moves by the system length L relative to the wall displacement of a single lattice distance αd. The displacement of the dislocation x_d relates to γ as $x_d = \gamma HL/\alpha d$. When $x_d = L$, we obtain $\gamma H/\alpha d = 1$. Differentiating $x_d = \gamma HL/\alpha d$ with respect to time and using relations $L = N_x\alpha d$ and $v_w = \dot{\gamma}H$, we obtain the simple relation $\dot{x}_d = v_d = N_x v_w$ as explained in Fig. 1. This consistency between our results and Orowan's theory confirms that the observed motion is indeed the dislocation glide. At $\mu \geq 0.15$, no continuous red line appears as crystal destruction impedes the dislocation glide [see Fig. 3(a)]. We quantify structure using the average contact number $\bar{Z}$ versus strain [see Fig. 3(c)]. At $\mu \lesssim 0.1$, $\bar{Z}$ remains near 6 even for large γ, indicating that the hexagonal order is stable under shear due to dislocation glide, as shown in Fig. 3(a). Conversely, at $\mu \gtrsim 0.15$, $\bar{Z}$ deviates from 6 with γ, signaling the hexagonal

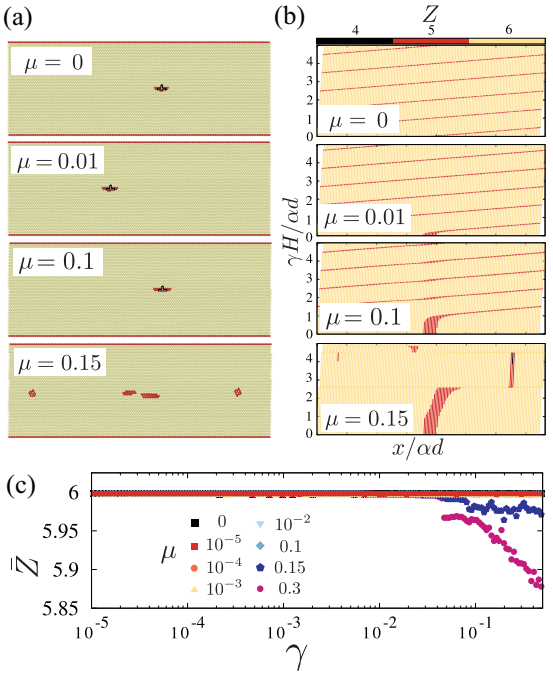

FIG. 3. (a) Snapshots at strain $\gamma \simeq 0.077$ ($\gamma H/\alpha d \simeq 4$) with various μ. Yellow particles have six contacts; red particles have fewer. Crystal order preserves at $\mu \lesssim 0.1$ due to dislocation glide. At higher μ, crystal order breaks and gliding ceases. Movies 1–4 in SM [36] show these dynamics. (b) Trajectories of $N_x + 1$ particles in the upper crystal, initially located at the interface. Horizontal and vertical axes represent the scaled particle positions $x/\alpha d$ and scaled strain $\gamma H/\alpha d$. Colors indicate the contact number Z. For $\mu \lesssim 0.1$, the red region moves straight with a displacement $x_d = \gamma HL/\alpha d$ relative to strain γ. This behavior corresponds to dislocation glide, which does not occur at $\mu \gtrsim 0.15$ due to crystal breakage. (c) Average contact number $\bar{Z}$ versus strain γ. $\bar{Z} = 6$ for perfect hexagonal structures, with deviations indicating crystal breakage. At $\mu \lesssim 0.1$, $\bar{Z}$ remains 6, indicating that the hexagonal structure is stable under shear. For $\mu \gtrsim 0.15$, $\bar{Z}$ decreases with γ, indicating the crystal breakage.

structure breakdown. These results demonstrate that the current setup exhibits dislocation glide at $\mu \lesssim 0.1$, which is the first observation of dislocation glide in frictional granular media.

Although primarily studying dislocation glide, we also briefly categorize friction-related plastic deformation in this system and note distinctions from amorphous systems. Movies 5–12 in SM [36] illustrate the large-strain behavior ($0 \leq \gamma \leq 5.3$) for systematically varied μ, simulated at an accelerated shear rate of $\dot{\gamma} = 10^{-2}\,\mathrm{s}^{-1}$ to reduce computation time. For $\mu = 0$, dislocation glide occurs at a very small strain. At $\mu = 0.1$, we observe friction-induced resistance to particle rearrangement at a small strain as shown in Fig. 3(b), a behavior characteristic of frictional granular media but absent in microcrystalline materials [1,8]. For μ slightly greater than 0.1, intermittent localized defect formation occurs distant from the initial dislocation. This localized, intermittent rearrangement would be analogous to avalanchelike plastic deformation in amorphous media [38,39]. However, the present system is crystalline; unlike amorphous systems, where (still debated) shear transformation zones [40] can act as localized weak spots, such explicit weak spots are not apparent here. For $\mu \gg 0.1$, crack growth initiates at original dislocation sites, and the fracture type seems to be mode I [41]. The crack angle is approximately $5\pi/6$, reflecting its crystalline nature, while a basic application of the maximum principal stress theory to our geometry $\sigma_{xx} \simeq \sigma_{yy}$ suggests an angle of approximately $3\pi/4$ [42]. Furthermore, with increasing strain, the entire system seems to progress toward a disordered state. At a sufficiently large μ and γ, once the crystal structure collapses, the system's behavior is no longer crystalline, and amorphous properties such as shear band [43] or power-law stress-drop statistics [38] would be observed.

The rheological behavior changes in response to structural changes induced by varying μ. We compute the normal and shear stresses, σ_{xx}, σ_{yy}, and σ_{xy}, based on the positions, velocities, and forces of particles [44,45] (see Eq. S5 in SM [36]). Figure 4(a) presents the logarithmic plot of scaled shear stress σ_{xy}/E versus strain γ. For reference, σ_{xy} of the frictionless perfect crystal ($N = N_x N_y$, $\alpha = 0.95$) is also presented. For all μ, linear responses ($\sigma_{xy} \propto \gamma$) are observed at small γ, followed by yielding at specific γ. The linear response regimes align well with that of the perfect crystal (see details in Fig. S1 in SM [36]). In the frictionless case ($\mu = 0$) with the dislocation, σ_{xy} exhibits extremely low yield stress (first peak in σ_{xy}) compared to that of the perfect crystal. This low yield stress originates from the small elastic barrier due to the dislocation, analogous to the atomic-scale Peierls stress [1,3–6,8], differing only in system length scale. For finite but small interparticle friction ($\mu \lesssim 0.1$), where dislocation glide occurs [see Fig. 3(a)], both yield stress and strain decrease monotonically as μ decreases. For high interparticle friction ($\mu \gtrsim 0.1$) where crystal breakage occurs, yield strains are approximately 5%, which is comparable to values typically reported in amorphous granular media [46]. Following conventions [47–49], Fig. S2 in SM [36] shows σ_{xy} normalized by the theoretical shear modulus of the perfect crystal, where the normalized yield stress ranges from 10^{-4} to 10^{-1}, consistent with prior research on atomic-scale dislocations [47–49].

Granular media typically exhibit dilatancy, or volume expansion under shear [50]. In our constant volume setup, dilatancy manifests as increasing $-\sigma_{yy}$ with strain γ, evident for $\mu \gtrsim 0.15$ in Fig. 4(b). The inset shows a similar trend for σ_{xx}. However, at low friction ($\mu \lesssim 0.1$), dilatancy disappears with σ_{yy} and σ_{xx} remaining constant. This absence of dilatancy can be intuitively understood, as the system deformation is relaxed by dislocation glide before the onset of dilatancy.

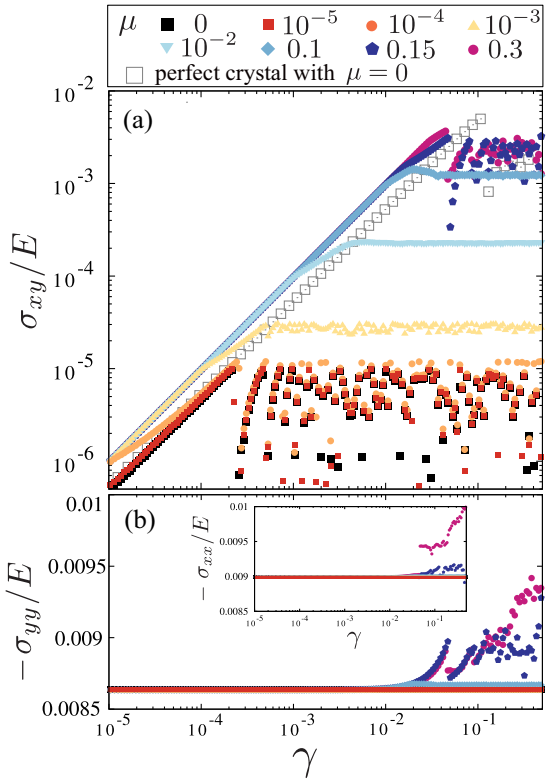

FIG. 4. Rheological responses at various μ. (a) Normalized shear stress σ_{xy}/E versus shear strain γ. The colored symbols present the data for the granular crystal with dislocation, and the open square presents data for the frictionless ($\mu = 0$) dislocation-free perfect crystal. Linear elastic behavior followed by yielding is observed in σ_{xy} vs γ for all μ. The yield stress (first peak in σ_{xy}) of the crystal with the dislocation decreases with decreasing μ and can be significantly lower than that of the perfect crystal. (b) Normalized normal stress $-\sigma_{yy}/E$ versus γ. The increase in $-\sigma_{yy}$ with γ, corresponding to dilatancy, is absent for small interparticle friction ($\mu \lesssim 0.1$) due to relaxation of the deformation via dislocation glide. The inset shows $-\sigma_{xx}/E$ vs γ, which also exhibits no dilatancy at $\mu \lesssim 0.1$.

Figure 5 presents the yield stress σ_Y of the crystal with dislocation versus μ, with σ_Y defined as the first peak in the σ_{xy} vs γ curve. For comparison, we include yield stress data for the perfect crystals ($N = N_x \times N_y$ particles, $\alpha = 0.95$) at various μ. At $\mu \lesssim 0.1$, σ_Y of the crystal with dislocation varies linearly with μ, which can be fitted by $\sigma_Y/E = 9.8 \times 10^{-6} + 1.5 \times 10^{-2}\mu$. For $\mu \gtrsim 0.1$, the data deviate from this linear relation as the crystal order breaks down and dislocation glide ceases [see Figs. 3(a)–3(c)]. Notably, dislocation glide reduces σ_Y significantly below the values of perfect crystals. As shown in Figs. 4(a) and 4(b), the shear stress σ_{xy}, normalized by $-\sigma_{yy} \sim 10^{-2}E$, ranges from 10^{-4} to 10^{-1}, which is significantly lower than typical values for amorphous granular media ($0.2 \lesssim -\sigma_{xy}/\sigma_{yy} \lesssim 0.6$ [46,50–53]). This marked difference arises from distinct yielding mechanisms. Dislocation glide

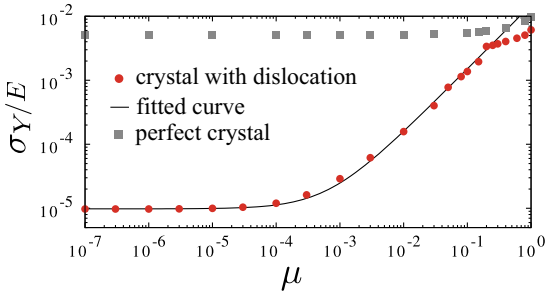

FIG. 5. Yield stress σ_Y of the crystal with dislocation, defined as the first peak in σ_{xy} vs γ, as a function of μ. Data for the perfect crystal with finite μ are included for comparison. Because of the dislocation glide, σ_Y of the crystal with the dislocation becomes significantly below the values of the perfect crystal. At $\mu \lesssim 0.1$, σ_Y of the crystal with a dislocation can be fitted by the linear function $\sigma_Y/E = 9.8 \times 10^{-6} + 1.5 \times 10^{-2}\mu$.

involves successive defect motion in crystalline media, whereas amorphous yielding proceeds via localized intermittent particle rearrangements [38,40]. The yielding in granular media is conventionally described by phenomenological models like Mohr-Coulomb [50] or Drucker-Prager [50,54] criteria, which do not address microscopic yielding mechanisms. The yielding mechanism in the current system with small μ is clearly identifiable as dislocation glide, making phenomenological descriptions unnecessary.

We consider a qualitative model to explain the result in Fig. 5. The linear relation between σ_Y and μ arises from the contributions of both elastic barrier and interparticle friction. In the frictionless case, the dislocation moves by overcoming the elastic barrier stress $\sigma_e(\sigma_{yy})$, which corresponds to the Peierls stress in atomic systems [1–9]. $\sigma_e(\sigma_{yy})$ generally depends on the normal stress σ_{yy} [55,56] (or lattice constant α), often with complex relations [57]. Despite extensive theoretical studies [1,3,5,8], precisely determining $\sigma_e(\sigma_{yy})$ remains challenging even for atomic crystals [58] (we examined the lattice constant effect and found a complex nonmonotonic dependence [59]). For frictional cases, we must account for interparticle friction, an effect absent in atomic crystals. Dislocation glide requires local rearrangement between contacting particles at the dislocation core. With friction present, particles must additionally overcome frictional constraints to rearrange. The normal stress in the system is approximately $|\sigma_{xx}|/E \simeq |\sigma_{yy}|/E \simeq 10^{-2}$ [Fig. 4(b)]. The local stress needed for particle rearrangement at the dislocation core can be estimated as $\mu|\sigma_{yy}| \simeq 10^{-2}\mu E$; the product of interparticle friction and normal stress. Combining the contributions from elastic barrier and interparticle friction provides the linear relation with respect to μ, $\sigma_Y \simeq \sigma_e(\sigma_{yy}) + \mu|\sigma_{yy}|$, consistent with our observations in Fig. 5.

In our system, finite friction induces qualitative changes in the yielding behavior. At low friction, dislocation glide

occurs. For intermediate μ, we observe intermittent defect formation. This intermittent localized rearrangement would be reminiscent of amorphous systems [38,40], a similarity that extends to the yield strain of approximately 5% [46]. At large friction $\mu \gg 0.1$, the system exhibits defect expansion from the initial dislocation. Understanding of the qualitative transition among the distinct yielding modes at a finite μ remains an open question. While formal analysis for yielding behavior via the friction-incorporating Jacobian matrix is possible for granular systems [60,61], extracting physical insights remains challenging.

Summary—We numerically investigated the structural and rheological responses of a granular crystal with a dislocation under slow shear. Our key findings are (i) the current granular system inspired by atomic-scale dislocation theory [1–6,8] exhibits dislocation glide for low interparticle friction ($\mu \lesssim 0.1$), as presented in Figs. 3(a)–3(c), whereas for large μ, the gliding behavior is absent due to crystal breakage; (ii) this gliding results in a significantly lower yield stress σ_Y than in perfect crystals (see Figs. 4 and 5) with σ_Y varying linearly with μ due to combined contributions from the elastic barrier associated with the Peierls stress and the interparticle friction. The experimental realization of the current setup is feasible in principle, though it requires meticulous preparation. Investigating screw dislocations, multidislocation systems, and dislocation creation or annihilation in granular media—well-established phenomena in atomic crystals [8]—presents promising directions. The low yield stress enabled by dislocation glide in granular media suggests a novel friction control approach, fundamentally different from conventional methods like ball bearings or fluid lubrication. This study bridges granular physics and atomic crystallography, offering interdisciplinary insights into materials science.

Acknowledgments—This work was supported by JSPS KAKENHI Grants No. JP24H00196, No. JP25K17359, No. JP24KJ0156. The authors also thank the Supercomputer Center, the Institute for Solid State Physics, the University of Tokyo for the use of the facilities (2025-Ba-0063).

Data availability—The data that support the findings of this Letter are openly available [62], embargo periods may apply.

[1] R. Peierls, Proc. Phys. Soc. London **52**, 34 (1940).
[2] F. R. N. Nabarro, Proc. Phys. Soc. **59**, 256 (1947).
[3] F. R. N. Nabarro, Philos. Mag. A **75**, 703 (1997).
[4] F. R. N. Nabarro, Mater. Sci. Eng. A **234–236**, 67 (1997).
[5] B. Joós and M. S. Duesbery, Phys. Rev. Lett. **78**, 266 (1997).
[6] B. Joós and J. Zhou, Philos. Mag. A **81**, 1329 (2001).
[7] J. N. Wang, Acta Mater. **44**, 1541 (1996).
[8] P. M. Anderson, J. P. Hirth, and J. Lothe, *Theory of Dislocations* (Cambridge University Press, Cambridge, England, 2017).
[9] H. B. Huntington, Proc. Phys. Soc. **68**, 1043 (1955).
[10] Y. N. Osetsky and D. J. Bacon, Model. Simul. Mater. Sci. Eng. **11**, 427 (2003).
[11] V. Bulatov and W. Cai, *Computer Simulations of Dislocations* (Oxford University Press, New York, 2006).
[12] N. J. Wagner, B. L. Holian, and A. F. Voter, Phys. Rev. A **45**, 8457 (1992).
[13] W. L. Bragg and J. F. Nye, Proc. R. Soc. A **190**, 474 (1947).
[14] W. L. Bragg and W. Lomer, Proc. R. Soc. A **196**, 171 (1949).
[15] W. Lomer, Proc. R. Soc. A **196**, 182 (1949).
[16] W. M. Lomer and J. F. Nye, Proc. R. Soc. A **212**, 576 (1952).
[17] D. Vecchiolla and S. L. Biswal, Soft Matter **15**, 6207 (2019).
[18] M. E. Rosa and M. A. Fortes, Philos. Mag. A **77**, 1423 (1998).
[19] A. N. Karuriya and F. Barthelat, Proc. Natl. Acad. Sci. U.S.A. **120**, e2215508120 (2023).
[20] A. Panaitescu, K. A. Reddy, and A. Kudrolli, Phys. Rev. Lett. **108**, 108001 (2012).
[21] M. Otsuki, H. Hayakawa, and S. Luding, Prog. Theor. Phys. **184**, 110 (2010).
[22] M. Otsuki and H. Hayakawa, Soft Matter **19**, 2127 (2023).
[23] M. Alam and S. Luding, Phys. Fluids **15**, 2298 (2003).
[24] A. Merkel and S. Luding, Int. J. Solids Struct. **106**, 91 (2017).
[25] A. Plati and A. Puglisi, Phys. Rev. Lett. **128**, 208001 (2022).
[26] P. A. Cundall and O. D. L. Strack, Géotechnique **29**, 47 (1979).
[27] R. D. Mindlin, J. Appl. Mech. **16**, 259 (2021).
[28] Y. Tsuji, T. Tanaka, and T. Ishida, Powder Technol. **71**, 239 (1992).
[29] T. Pöschel and N. V. Brilliantov, *Granular Gas Dynamics* (Springer, Berlin, 2003).
[30] S. Luding, Granular Matter **10**, 235 (2008).
[31] L. E. Silbert, D. Ertaş, G. S. Grest, T. C. Halsey, D. Levine, and S. J. Plimpton, Phys. Rev. E **64**, 051302 (2001).
[32] J. S. Marshall, J. Comput. Phys. **228**, 1541 (2009).
[33] A. P. Thompson, H. M. Aktulga, R. Berger, D. S. Bolintineanu, W. M. Brown, P. S. Crozier, P. J. in't Veld, A. Kohlmeyer, S. G. Moore, T. D. Nguyen *et al.*, Comput. Phys. Commun. **271**, 108171 (2022).
[34] W. D. Callister Jr and D. G. Rethwisch, *Materials Science and Engineering: An Introduction* (John wiley & sons, London, 2020).
[35] C. G. Robertson, R. Bogoslovov, and C. M. Roland, Phys. Rev. E **75**, 051403 (2007).
[36] See Supplemental Material at http://link.aps.org/supplemental/10.1103/7g7s-c157 for simulation details, additional analyses, and simulation movies.
[37] A. Lunev, A. Y. Kuksin, and S. Starikov, Int. J. Plast. **89**, 85 (2017).
[38] D. Houdoux, A. Amon, D. Marsan, J. Weiss, and J. Crassous, Commun. Earth Environ. **2**, 1 (2021).
[39] M. Nicolson, in *Mathematical Proceedings of the Cambridge Philosophical Society* (Cambridge University Press, Cambridge, England, 1949), Vol. 45, pp. 288–295.

[40] A. Nicolas, E. E. Ferrero, K. Martens, and J.-L. Barrat, Rev. Mod. Phys. **90**, 045006 (2018).
[41] N. Perez, *Fracture Mechanics*, 2nd ed. (Springer International Publishing, Cham, Switzerland, 2016).
[42] A. P. Boresi and R. J. Schmidt, *Advanced Mechanics of Materials* (John Wiley & Sons, New York, 2002).
[43] S. Mandal, M. Nicolas, and O. Pouliquen, Phys. Rev. X **11** (2021).
[44] M. P. Allen and D. J. Tildesley, *Computer Simulation of Liquids*, 2nd ed. (Oxford University Press, Oxford, 2017).
[45] D. J. Evans and G. P. Morriss, *Statistical Mechanics of Nonequilibrium Liquids*, 2nd ed. (Cambridge University Press, Cambridge, England, 2008).
[46] J. Desrues and G. Viggiani, Int. J. Numer. Anal. Methods Geomech. **28**, 279 (2004).
[47] K. Gouriet, P. Carrez, and P. Cordier, Model. Simul. Mater. Sci. Eng. **22**, 025020 (2014).
[48] Y. Kamimura, K. Edagawa, A. M. Iskandarov, M. Osawa, Y. Umeno, and S. Takeuchi, Acta Mater. **148**, 355 (2018).
[49] K. Edagawa, Y. Kamimura, A. M. Iskandarov, Y. Umeno, and S. Takeuchi, Materialia **5**, 100218 (2019).
[50] B. Andreotti, Y. Forterre, and O. Pouliquen, *Granular Media: Between Fluid and Solid* (Cambridge University Press, Cambridge, England, 2013).
[51] A. Taboada, N. Estrada, and F. Radjaï, Phys. Rev. Lett. **97**, 098302 (2006).
[52] P.-E. Peyneau and J.-N. Roux, Phys. Rev. E **78**, 011307 (2008).
[53] W.-T. Yeh, M. Ozawa, K. Miyazaki, T. Kawasaki, and L. Berthier, Phys. Rev. Lett. **124**, 225502 (2020).
[54] D. C. Drucker and W. Prager, Q. Appl. Math. **10**, 157 (1952).
[55] J. D. Clayton, *Nonlinear Mechanics of Crystals* (Springer, Dordrecht, 2010).
[56] J. O. Chua and A. L. Ruoff, J. Appl. Phys. **46**, 4659 (1975).
[57] G. Liu, X. Cheng, J. Wang, K. Chen, and Y. Shen, Int. J. Plast. **90**, 156 (2017).
[58] Y. Kamimura, K. Edagawa, and S. Takeuchi, Acta Mater. **61**, 294 (2013).
[59] F. Nakai, T. Uneyama, Y. Sasaki, K. Yoshii, and H. Katsuragi, arXiv:2505.12042.
[60] D. Ishima, K. Saitoh, M. Otsuki, and H. Hayakawa, Phys. Rev. E **107**, 034904 (2023).
[61] D. Ishima, K. Saitoh, M. Otsuki, and H. Hayakawa, Phys. Rev. E **107**, 054902 (2023).
[62] F. Nakai, T. Uneyama, Y. Sasaki, K. Yoshii, and H. Katsuragi, Dataset for "Dislocation Glides in Granular Media," Version v1, Zenodo (2025), 10.5281/zenodo.14942701.